JACS
JOURNAL OF THE AMERICAN CHEMICAL SOCIETY
Article
pubs.acs.org/JACS

Isolation of a Mixed Valence Diiron Hydride: Evidence for a Spectator Hydride in Hydrogen Evolution Catalysis

Wenguang Wang,[†] Mark J. Nilges,[†] Thomas B. Rauchfuss,*[,†] and Matthias Stein*[,‡]

[†]School of Chemical Sciences, University of Illinois, Urbana, Illinois 61801, United States

[‡]Max Planck Institute for Dynamics of Complex Technical Systems, Sandtorstraβe 1, 39106 Magdeburg, Germany

Supporting Information

ABSTRACT: The mixed-valence diiron hydrido complex (μ-H)Fe_2(pdt)$(CO)_2$(dppv)$_2$ ([H**1**]^0, where pdt =1,3-propanedithiolate and dppv = *cis*-1,2-$C_2H_2(PPh_2)_2$), was generated by reduction of the differous hydride [H**1**]$^+$ using decamethylcobaltocene. Crystallographic analysis shows that [H**1**]^0 retains the stereochemistry of its precursor, where one dppv ligand spans two basal sites and the other spans apical and basal positions. The Fe---Fe bond elongates to 2.80 from 2.66 Å, but the Fe−P bonds only change subtly. Although the Fe−H distances are indistinguishable in the precursor, they differ by 0.2 Å in [H**1**]^0. The X-band electron paramagnetic resonance (EPR) spectrum reveals the presence of two stereoisomers, the one characterized crystallographically and a contribution of about 10% from a second symmetrical (*sym*) isomer wherein both dppv ligands occupy apical−basal sites. The unsymmetrical (*unsym*) arrangement of the dppv ligands is reflected in the values of $A(^{31}P)$, which range from 31 MHz for the basal phosphines to 284 MHz for the apical phosphine. Density functional theory calculations were employed to rationalize the electronic structure of [H**1**]^0 and to facilitate spectral simulation and assignment of EPR parameters including ^1H and ^{31}P hyperfine couplings. The EPR spectra of [H**1**]^0 and [D**1**]^0 demonstrate that the singly occupied molecular orbital is primarily localized on the Fe center with the longer bond to H, that is, Fe^{II}−H···Fe^{I}. The coupling to the hydride is $A(^1H)$ = 55 and 74 MHz for *unsym*- amd *sym*-[H**1**]^0, respectively. Treatment of [H**1**]^0 with H^+ gives 0.5 equiv of H_2 and [H**1**]$^+$. Reduction of D^+ affords D_2, leaving the hydride ligand intact. These experiments demonstrate that the bridging hydride ligand in this complex is a spectator in the hydrogen evolution reaction.

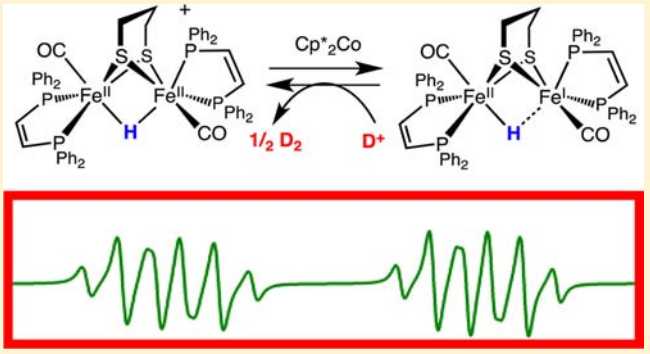

INTRODUCTION

Reflecting interest in sustainable fuels and energy storage,[1,2] the hydrogen evolution reaction (HER) is receiving intense attention. Metallic platinum is a prominent catalyst for the HER, although commercial electrolyzers rely on nickel oxides.[3] Interest in the HER has led to a focus on hydrogenase enzymes and related bioinspired catalysts.[4] Because of their relationship to active sites of the hydrogenases, Fe−S−CO ensembles have been of particular interest.[5] These clusters are redox active, but unlike traditional high-spin Fe−S clusters, they are low spin species and form hydride derivatives, as seems to be required for metal-catalyzed hydrogen evolution and uptake.

Guided by the crystallographic characterization of two main families of hydrogenases, catalysts have been developed that resemble their active sites to varying extents. Although modest progress has been reported for functional mimics of the [NiFe]−H_2ases,[6] hundreds of catalysts have been developed based on the active site of the [FeFe]−H_2ases.[7,8] These catalysts are of the type $Fe_2(SR)_2(CO)_{6-x}L_x$, although only a few exhibit high rates or low overpotentials[9] and none exhibits both.[10] Generally, these catalysts can be classified according to their HER mechanism. The CO-rich diiron compounds, for example, $Fe_2(SR)_2(CO)_6$, are poor bases and thus resist protonation. These species do however reduce at relatively mild potentials (about −1.65 V, all couples vs $Fc^{+/0}$ in MeCN solution, about −1 V vs the standard hydrogen electrode), and the resulting anionic Fe(I)Fe(0) or Fe(0)Fe(0) species protonate readily thereby initiating the HER.[10,11] Reductions can be achieved at a cathode[12] or in photosensitized systems by electron transfer from a high potential donor such as $[Ru(bipy)_3]^+$ ($E^1/_2$ = −1.69 V).[13] The second major class of bioinspired HER catalysts are donor-ligand-substituted diiron(I) dithiolates, which are sufficiently basic that they undergo direct protonation at the Fe−Fe bond.[5,14] This protonation produces cationic diferrous μ-hydrides that are susceptible to reduction and subsequent protonation resulting in the HER.[7,15] A third family of bioinspired HER catalysts, which appear to be truly biomimetic, also feature some donor ligands in place of CO, but they undergo protonation at a *single* Fe center, usually mediated by an amine cofactor.[9,16]

Received: December 20, 2012
Published: February 5, 2013

   dx.doi.org/10.1021/ja312458f | *J. Am. Chem. Soc.* 2013, 135, 3633−3639

All diiron-based HER catalysts operate by the intermediacy of mixed valence hydrides, an otherwise rare class of complexes.[11,17] These S = $^1/_2$ species often arise by protonation of mixed valence Fe(I)Fe(0) species (eqs 1 and 2):

$$[Fe^{I}Fe^{I}] + e^{-} \rightarrow [Fe^{0}Fe^{I}]^{-} \quad (1)$$

$$[Fe^{0}Fe^{I}]^{-} + H^{+} \rightarrow [HFe^{II}Fe^{I}] \quad (2)$$

Alternatively, similar mixed valence hydrides are also produced by 1 e^- reduction of diferrous hydrides (eqs 3 and 4):[10,11]

$$[Fe^{I}Fe^{I}] + H^{+} \rightarrow [HFe^{II}Fe^{II}]^{+} \quad (3)$$

$$[HFe^{II}Fe^{II}]^{+} + e^{-} \rightarrow [HFe^{II}Fe^{I}] \quad (4)$$

These two schemes highlight the centrality of the hydride derivatives of $Fe^{II}Fe^{I}$ centers. Reduction enhances the susceptibility of hydride complexes toward protonolysis to give H_2.[15,18] Related to the HER process, S = $^1/_2$ diiron hydrides have been generated in situ and characterized by electron paramagnetic resonance (EPR) spectroscopy. Specifically, the hydrides $[HFe_2(SH)_2(CO)_6]^0$, $[HFe_2(pdt)(CO)_4(PMe_3)_2]^0$, and $[HFe_2(edt)(CO)_4(PMe_3)_2]^0$ display EPR signals centered near g = 2.007, with the unpaired electron spin exhibiting coupling to the nuclear spin of the bridging hydride and other ligands on these diiron centers (edt^{2-} = $C_2H_4S_2^{2-}$, pdt^{2-} = $C_3H_6S_2^{2-}$).[2,19] In the present work, we have isolated analytically pure samples of the related mixed valence hydride $[HFe_2(pdt)(CO)_2(dppv)_2]^0$ ([H**1**]^0, dppv = *cis*-1,2-$C_2H_2(PPh_2)_2$).[9] In addition to being a source of crystallographic and spectroscopic information, this S = $^1/_2$ mixed-valence radical provides an opportunity to probe more deeply within the catalytic cycle for the reduction of protons to dihydrogen.

RESULTS

Reduction of Diferrous Hydrides. Redox properties were evaluated for three diiron hydrides of differing basicities, redox potentials, and steric bulk (Figure 1). The cyclic voltammograms of $[HFe_2(pdt)(CO)_4(dppv)]BF_4$ ([H**3**]$^+$), $[HFe_2(pdt)(CO)_3(dppv)(PMe_3)]BF_4$ ([H**2**]$^+$), and $[HFe_2(pdt)(CO)_2(dppv)_2]BF_4$ ([H**1**]$^+$) in THF–Bu_4NPF_6 exhibit a range of reduction potentials each with differing reversibility. Upon replacing CO with phosphine ligands in this series of complexes, the reduction potentials shift to more negative values from −1.27 V for [H**3**]$^{+/0}$ to −1.62 V for [H**2**]$^{+/0}$ and −1.77 V for [H**1**]$^{+/0}$. As indicated in Figure 1, the redox event becomes more reversible for the more demanding reductions, as reflected by changes in i_{pc}/i_{pa} from 0.52 to 0.99. These results suggested that [H**1**]^0 should be sufficiently stable to allow isolation.

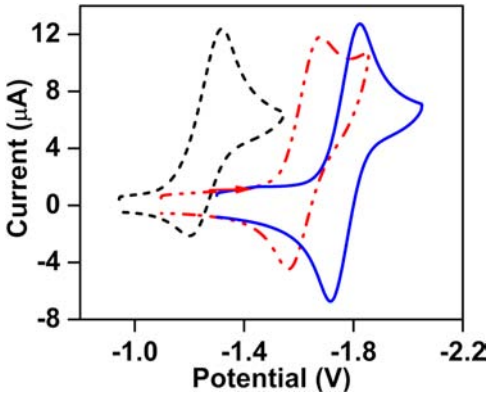

Figure 1. Cyclic votammograms for $[HFe_2(pdt)(CO)_2(dppv)_2]BF_4$ (solid line), $[HFe_2(pdt)(CO)_3(dppv)(PMe_3)]BF_4$ (dash-dot line), and $[HFe_2(pdt)(CO)_4(dppv)]BF_4$ (dashed line) couples. Conditions: 10 mM sample in THF, 0.1 M Bu_4NPF_6; scan rate, 100 mV s^{-1}; potentials vs $Fc^{+/0}$. Results: $E^1/_2$[H**1**]$^{+/0}$ = −1.77 V, i_{pc}/i_{pa} = 0.99; $E^1/_2$[H**2**]$^{+/0}$ = −1.62 V, i_{pc}/i_{pa} = 0.72; $E^1/_2$[H**3**]$^{+/0}$ = −1.27 V, i_{pc}/i_{pa} = 0.52.

Reduction of [H**1**]$^+$ with decamethylcobaltocene (Cp_2*Co, $E^1/_2$ = −1.94 V in CH_2Cl_2[20]) afforded the targeted complex [H**1**]^0 (Scheme 1). The conversion is signaled by a change in the color of the THF solution from brown to black. After evaporating the reaction mixture, the product was extracted into toluene and precipitated by pentane. Black microcrystals of [H**1**]^0 are stable in the absence of air.

Scheme 1

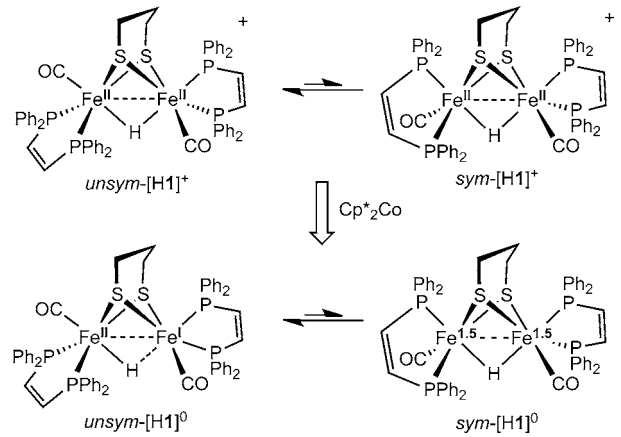

The IR spectrum of [H**1**]^0 exhibits a strong ν_{CO} band at 1893 cm^{-1}, which is shifted by 57 cm^{-1} to lower energy compared to ν_{CO} for [H**1**]BF_4. The magnitude of the shift in ν_{CO} is in line with density functional theory (DFT) calculations (Supporting Information), which predict a shift of 46 cm^{-1}. One electron reduction of $[HFe_2(pdt)(CO)_4(PMe_3)_2]^+$ shifts ν_{COavg} by 80 cm^{-1}.[2] Treatment of [H**1**]^0 with one equiv of $FcBF_4$ gave back [H**1**]$^+$ (Figure 2).

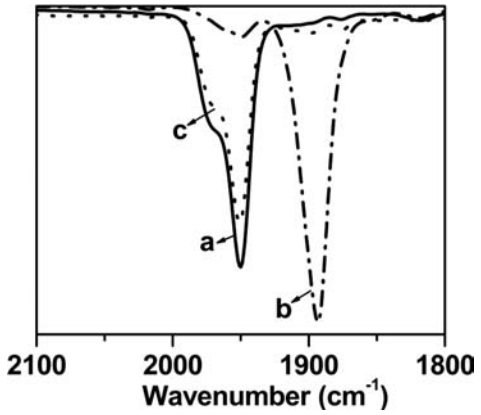

Figure 2. IR spectra in ν_{CO} region for [H**1**]BF_4 in THF solution (a), the same solution after treatment with Cp^*_2Co (b), and oxidation of this solution with 1 equiv of solid $[Cp_2Fe]BF_4$ (c).

dx.doi.org/10.1021/ja312458f | J. Am. Chem. Soc. 2013, 135, 3633−3639

Crystallographic Characterization of $HFe_2(pdt)(CO)_2(dppv)_2$. The considerable stability of $[H1]^0$ allowed us to grow single crystals suitable for X-ray diffraction. Crystallographic analysis reveals a neutral complex of the type $Fe_2(SR)_2L_6(\mu\text{-}X)$. The framework is similar to *unsym*-$[H1]^+$ in that one dppv is chelated to the two dibasal sites on Fe(1) and the other dppv spans apical−basal positions on Fe(2).[21] Relative to $[H1]^+$, the Fe---Fe distance in $[H1]^0$ is longer by 0.138 Å (Table 1). The Fe−S bonds are also elongated by approximately 0.05 Å. The hydride ligand was located in the difference map, and its position and isotropic displacement parameters were refined. In $[H1]^+$, the hydride ligand is approximately equidistant between two iron centers, whereas in $[H1]^0$, the hydride ligand is semibridging, with the Fe−H distances differing by 0.21 Å. The location of the hydride ligands is consistent with the results of DFT calculations (see below). Another striking difference is the elongation of the Fe(2)−P_{apical} bond by 0.07 Å. Overall, the crystallographic data indicate that Fe(2) is more reduced than Fe(1).

Table 1. Bond Distances (Å) in *unsym*-$[H1]BF_4$[a] and *unsym*-$[H1]^0$

bond	$[H1]^+$	$[H1]^0$
Fe(1)−Fe(2)	2.6646(6)	2.8030(5)
Fe(1)−H	1.65(3)	1.61(2)
Fe(2)−H	1.68(3)	1.82(3)
Fe(1)−C	1.739(4)	1.780(2)
Fe(2)−C	1.780(3)	1.746(2)
Fe(1)-S_{avg}	2.262	2.311
Fe(2)−S_{avg}	2.2736	2.3167
Fe(1)−P_{avg}	2.2336	2.1892
Fe(2)−P_{basal}	2.236(9)	2.2264(7)
Fe(2)−P_{apical}	2.2287(9)	2.3039(7)

[a]Taken from ref 21.

EPR Characterization of $HFe_2(pdt)(CO)_2(dppv)_2$ and DFT Analysis. The X-band EPR spectrum of a fluid (toluene at −30 °C) solution of $[H1]^0$ exhibits a rich set of couplings (Figure 4 and Table 2). Digital simulation of the spectrum indicates the presence of two S = $^1/_2$ species in the ratio of 85:15, the same isomer ratio seen for $[H1]^+$.[9] The subspectrum from the major isomer is dominated by a hyperfine interaction of 284 MHz that is proposed to originate from the unique apical phosphine ligand on Fe(2) of *unsym*-$[H1]^0$. The unique phosphorus donor is attached to the center of greater Fe(I) character (see below). The remaining hyperfine splittings can be simulated by couplings to four I = $^1/_2$ centers, originating from the three basal phosphines ($A(^{31}P)_{basal}$ ~31 MHz) and the hydride ($A(^1H)$ = 55 MHz). For comparison, in $[HFe_2(pdt)(CO)_4(PMe_3)_2]^0$, $A_{iso}(^{31}P)_{basal}$ is 41.7 MHz (absolute values given for A_{iso}).[2] The EPR spectrum of $[H1]^0$ also consists a second subspectrum, originating from the symmetrical isomer of $[H1]^0$, which shows coupling to two apical phosphorus centers, $A(^{31}P)_{apical}$ = 228 and 192 MHz, and two basal phosphorus centers, ~30 MHz (Figure 4). Compared to the *unsym* isomer, the hydride displays a larger hyperfine interaction with $A(^1H)$ = 74 MHz. In $[HFe_2(SH)_2(CO)_6]^0$ and $[HFe_2(pdt)(CO)_4(PMe_3)_2]^0$, $A_{iso}(^1H)$ values are 90.8 and 75.8 MHz, respectively, which are comparable to that in *sym*-$[H1]^0$.[2,19] The difference in the *A* values for the apical versus basal P atoms indicates that the singly occupied molecular orbital (SOMO) is mainly localized at the two iron nuclei with

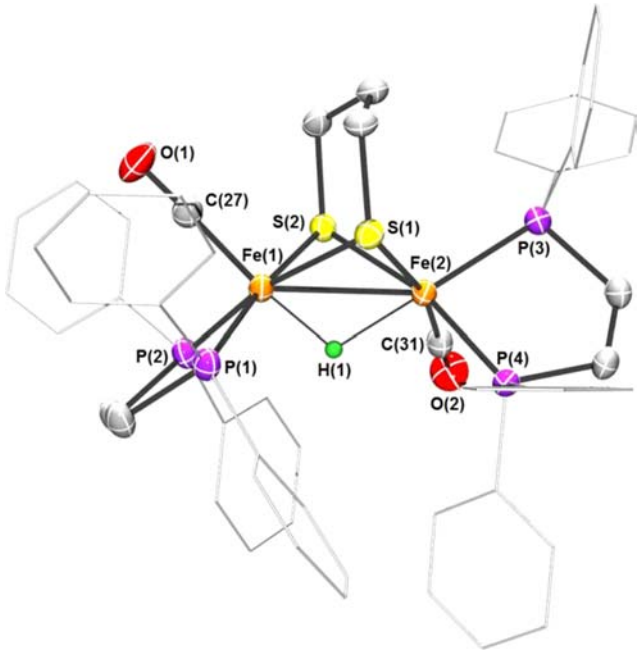

Figure 3. Structure of *unsym*-$[H1]^0$. Thermal ellipsoids are set at the 50% probability level. For clarity, phenyl groups are drawn as lines, and hydrogen atoms (except the hydride ligand) are omitted.

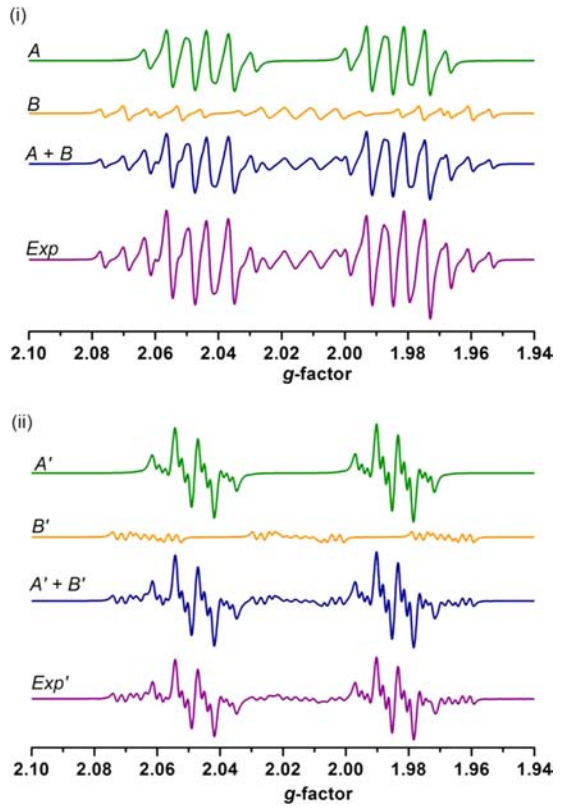

Figure 4. X-band EPR spectra for toluene solutions of $[H1]^0$ (i) and $[D1]^0$ (ii) at −30 °C in toluene with simulation of *unsym*-$[H1]^0$ (A); simulation of *sym*-H1 (B); simulation of a mixture of *unsym*- and *sym*-$[H1]^0$ (A + B); experimental spectrum of the mixture of $[H1]^0$ (exp); simulation of *unsym*-$[D1]^0$ (A′); simulation of *sym*-$[D1]^0$ (B′); simulation of $[D1]^0$ (A′ + B′); experimental spectrum of $[D1]^0$ (exp′).

dx.doi.org/10.1021/ja312458f | J. Am. Chem. Soc. 2013, 135, 3633−3639

Table 2. EPR Parameters for *unsym*- and *sym*-$[H1]^0$ and $[D1]^0$ from Simulations[a]

compd	*g* factor[b]	$A(^{31}P_{apical})$[c]	$A(^{31}P_{basal})$[c]	$A(^{1}H)$[c]	$A(^{2}H)$[c]
unsym-$[H1]^0$	2.003, 2.015, 2.026	284	32, 31, 31	55	–
sym-$[H1]^0$	2.002, 2.010, 2.021	228, 192	33, 30	74	–
unsym-$[D1]^0$	2.003, 2.015, 2.026	288	32, 31, 31	–	8.5
sym-$[D1]^0$	2.002, 2.010, 2.021	232, 194	34, 30	–	11.6

[a]See Figure 4. [b]*g* tensors were obtained by simulations of EPR spectra of the frozen sample (Supporting Information). [c]Isotropic hyperfine coupling constant (absolute value) in MHz also obtained by simulation. The differences in the *A* values between the spectra for $[H1]^0$ vs $[D1]^0$ are within the experimental uncertainty of ±3 MHz.

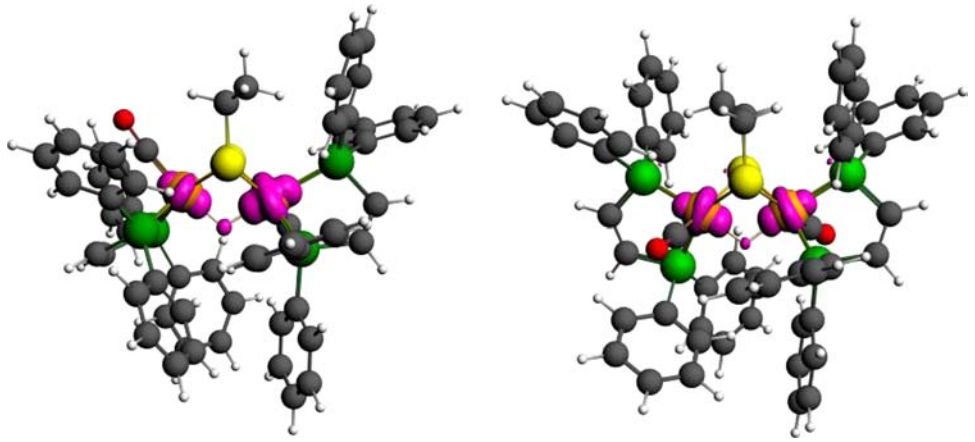

Figure 5. Unpaired spin density distribution in $HFe_2(pdt)(CO)_2(dppv)_2$ with isocontour plots at 0.005 e^-/a_0^3 (violet). Atomic spin populations for *unsym*-$[H1]^0$ (left): Fe(1) 0.32, Fe(2) 0.64, H −0.03, P_{apical} 0.053, P_{basal} 0.001, −0.003, and −0.01. For *sym*-$[H1]^0$ (right): Fe 0.36 and 0.39, H −0.02, P_{apical} 0.06 and 0.07, P_{basal} 0.01 and 0.003.

lobes of the orbitals pointing toward the apical binding sites. Phosphorus nuclei in the basal orientation are thus orthogonal to the SOMO and acquire less spin density.

The EPR spectrum of the deuteride $[D1]^0$ was also examined. The phosphorus couplings relative to $[H1]^0$ are unchanged. The small 1:1:1 deuterium splitting can be clearly observed (Figure 4ii). The $A(^2H)$ values are 8.5 and 11.6 MHz for *unsym*- and *sym*-D**1**, respectivly. These diminished hyperfine couplings agree with the diminished nuclear *g* factor for deuterium: g_H/g_D = 6.514.

DFT Calculations. DFT caculations are in agreement with experimental findings and yield a more rhombic *g* tensor for *unsym*-$[H1]^0$ (2.002, 2.005, 2.020) than for *sym*-$[H1]^0$ (2.002, 2.009, 2.011). The calculated atomic spin populations show that 96% of the unpaired spin in the *unsym*-$[H1]^0$ resides on the Fe centers with 0.32 e^- on Fe(1) and 0.64 e^- on Fe(2) (see Figure 3 for atom numbering). The apical phosphorus center on Fe(2) accounts for 5.3% of the calculated unpaired spin, whereas the other three P_{basal} centers contribute approximately 1%. The apical P ligand gives rise to a large hyperfine interaction with A_{iso} of +302 MHz while the isotropic ^{31}P hyperfine interactions of the basal P ligands are −11 to −30 MHz. The calculations on *unsym*-$[H1]^0$ support the assignment of unpaired electron spin mostly residing on Fe(2) as reflected in the large ^{31}P hyperfine interaction for the apical P atom (see Figure 5).

In *sym*-$[H1]^0$, the unpaired electron is almost equally distributed over the two iron atoms with atomic spin populations of 0.36 and 0.39. Thus, they bear a total of 75% unpaired spin density; the two apical phosphorus ligands can acquire 7% each, reflected in their large isotropic hyperfine interactions of +165 and +202 MHz. The two basal phosphines only carry 1.3% of the unpaired spin. Compared to $[HFe_2(pdt)(CO)_4(PMe_3)_2]^0$ where 0.3% unpaired spin density resides on the bridging hydride, in $[H1]^0$, the hydride ligand carries −0.03 e^- (unsym) and −0.02 e^- (sym).

In Gibbs free energies, *sym*-$[H1]^0$ is less stable than *unsym*-$[H1]^0$ by 4 kcal/mol (BP86-D) and 1 kcal/mol (B3LYP-D). The 0.15:0.85 distribution estimated from EPR analysis corresponds to a ΔG value of 0.8 kcal/mol at −30 °C. Structural changes upon reduction of $[H1]^+$ to $[H1]^0$ are well reproduced in the calculations (see Table 1 and the Supporting Information). The reduction potential of $[H1]^{+/0}$ was calculated to be −2.7 V compared to $Fc^{+/0}$ in the gas phase and −2.0 V using a COSMO solvation model. The latter value agrees well with the measured value of −1.8 V.[9] The calculated EPR parameters agree well with the experimentally determined ones (see the Supporting Information) and allow an assignment of nuclei and signs of hyperfine interactions in the experimental EPR spectra.

Reactions of $[HFe_2(pdt)(CO)_2(dppv)_2]$. Complex $[H1]^+$ is an electrocatalyst for the HER in the presence of strong acids. The catalytic current is observed at −2.1 V versus $Fc^{+/0}$, which corresponds to the $[H1]^{+/0}$ couple.[9] As the intermediate in this catalytic process, $[H1]^0$ was tested for its competency to reduce protons. As expected, $[H1]^0$ was found to react readily with strong acids with evolution of H_2. However, the details of this reaction proved to be surprising. Upon addition of 1.1 equiv of $H(OEt_2)_2BArF_4$ to THF solution of $[H1]^0$, the color immediately changed to brown red from black. The exclusive organometallic product (94% isolated yield) was $[H1]^+$, as verified by IR, and ^1H and $^{31}P\{^1H\}$ NMR analyses. It is known that $[H1]^+$ exists as two isomers that interconvert slowly, but reduction followed by oxidation with H^+ did not affect this ratio. Acids that are weaker than $H(OEt_2)_2BArF_4$, NH_4PF_6, and CF_3CO_2H, with pK_a^{MeCN} values of 8 and 12,[22] respectively, also

dx.doi.org/10.1021/ja312458f | J. Am. Chem. Soc. 2013, 135, 3633−3639

led to rapid evolution of H_2 from $[H1]^0$. We found however that $[H1]^0$ is unreactive toward benzoic acid, $pK_a^{MeCN} = 20.7$.

Yields of H_2 approached 50% relative to the amount of $[H1]^0$ (three experiments, standard deviation of 0.035). Upon treating $[H1]^0$ with $D(Et_2O)_2BArF_4$, the organoiron product was exclusively $[H1]^+$. The yield of $[H1]^+$ was quantified using the very stable salt $[HFe_2(edt)(CO)_4(PMe_3)_2]PF_6$ as an integration standard for NMR analysis. The ratio of $[H1]^+$ to $[HFe_2(edt)(CO)_4(PMe_3)_2]^+$ was found to be close to 1:1 by integration of the corresponding μ-H signals, thus confirming that no $[D1]^+$ was produced, whereas only $[D1]^+$ was produced in the reaction of $[D1]$ and $H(Et_2O)_2BArF_4$, as confirmed by ^2H, ^1H, and ^{31}P NMR analyses (Supporting Information). These results are summarized in eq 5 and 6:

$$HFe_2(pdt)(CO)_2(dppv)_2 + H^+ \rightarrow [HFe_2(pdt)(CO)_2(dppv)_2]^+ + 0.5H_2 \quad (5)$$

$$HFe_2(pdt)(CO)_2(dppv)_2 + D^+ \rightarrow [HFe_2(pdt)(CO)_2(dppv)_2]^+ + 0.5D_2 \quad (6)$$

In an effort to identify the nucleophilic site on the diiron complex, we examined the reaction of $[H1]^0$ with CF_3SO_3Me, expecting to generate an S-methylated radical cation $[H1Me]^+$. S-Alkylation of diferrous dithiolates has been demonstrated previously.[23] However, the reaction of $[H1]^0$ and CF_3SO_3Me in toluene also produced $[H1]^+$ with high yields. Gas chromatographic analysis of the volatile products revealed small amounts of methane, but the mass balance was poor.

DISCUSSION AND CONCLUSIONS

The new diiron hydride $[HFe_2(pdt)(CO)_2(dppv)_2]^0$ represents a sterically stabilized analogue of the mixed-valence hydride complexes invoked in many biomimetic HER processes.[7,8,10,11,17] The low symmetry of the main isomer of $[H1]^0$ allowed the analysis of the distribution of the SOMO over the nuclei in the core of the complex. Specifically, the Fe center with the stronger interaction with the hydride ligand is less reduced than the other Fe center. This observation is consistent with the destabilizing influence of hydrides on very low oxidation states, as is indicated by various ligand electronic parameters.[24] The result implies that reduction of diferrous complexes containing terminal hydride ligands, as required for the HER,[9] would occur at the nonhydride site.

Despite the ubiquity of iron hydrides and their mechanistic centrality, radical hydrides of iron are rare.[2,19,25] Two examples of ferric hydrides are $[Cp^*Fe(dppe)H]^+$ and $L_3Fe(\mu\text{-}NH)(\mu\text{-}H)FeL_3$ ($L_3 = [PhB(CH_2PPh_2)_3]^-$).[26] Crystallographically characterized iron(I) hydrides include $HFe(dppe)_2$ and the $S = {}^3/_2$ species $[(NacNac)FeH]^-$ (dppe = 1,2-$C_2H_4(PPh_2)_2$, NacNac = 2,2,6,6-tetramethyl-3,5-bis(2,6-diisopropylphenylimido)heptyl).[27]

As d^7–d^6 systems featuring bridging hydrides and two thiolates, $[H1]^0$ and the active site of the [NiFe]–hydrogenases ("Ni–C" state) are potentially related. The EPR parameters however suggest that the present NiFe system and the present FeFe hydride are quite different. EPR and ENDOR spectra for the NiFe enzyme from *Desulfovibrio vulgaris* Miyazaki F and *Ralstonia eutropha* reveal a small isotropic hyperfine couplings constant $A_{iso} \sim -3.5$ MHz for the bridging hydride.[28] In these cases, the SOMO is mainly localized on the Ni $3d_{z^2}$ orbital, which is perpendicular to the Ni---H vector.[29]

$[H1]^0$ has been previously implicated as an intermediate in hydrogen evolution catalyzed by $[H1]^+$. The new insights into the fact that it operates using a spectator hydride ligand provides a suitable opportunity to summarize current mechanistic schemes. As mentioned in the Introduction, two broad pathways exist for the HER by bioinspired diiron complexes, depending on the initiating reaction: reduction for the hexacarbonyls (mainly) vs protonation for substituted complexes.[10,11] Catalytic cycles initiated by protonation are always followed by reduction of the diferrous hydrides to give mixed-valence hydrides ($HFe^{II}Fe^{I}$). The subsequent step in the HER can be classified according to four subpathways, beginning with a bimolecular pathway that is independent of $[H^+]$ (eq 7):

$$2[HFe^{II}Fe^{I}] \rightarrow 2[Fe^{I}Fe^{I}] + H_2 \quad (7)$$

The poor reversibility for the couple $[HFe_2(pdt)(CO)_4(PMe_3)_2]^{0/+}$,[30] $[HFe_2(pdt)(CO)_3(dppv)(PMe_3)]^{0/+}$, and $[HFe_2(pdt)(CO)_4(dppv)]^{0/+}$ is attributed to this process. Three proton-induced pathways can also be envisioned for the HER (eq 8–10):

$$[HFe^{II}Fe^{I}] + H^+ \rightarrow [Fe^{II}Fe^{I}]^+ + H_2 \quad (8)$$

$$[HFe^{II}Fe^{I}] + [HFe^{II}Fe^{II}]^+ \rightarrow [Fe^{II}Fe^{I}]^+ + [Fe^{I}Fe^{I}] + H_2 \quad (9)$$

$$2[HFe^{II}Fe^{I}] + 2H^+ \rightarrow 2[HFe^{II}Fe^{II}]^+ + H_2 \quad (10)$$

In the case of $[H1]^0$, both the stoichiometry and deuterium labeling show that the μ-hydride ligand is a spectator, implicating the new process in eq 10. The dominance of this pathway reflects the bulky nature of $[H1]^0$.

Aside from the fact that the HER requires protonation of this mixed-valence species, mechanistic details are uncertain. Protonation of highly reduced compounds can trigger intermetallic electron transfer leading to the HER.[31] Protonation of $[H1]^0$ at Fe would afford a Fe(II)Fe(III) dihydride $[HH1]^+$, whereas S-protonation[5,32] of $[H1]^0$ would preserve the oxidation states.

EXPERIMENTAL SECTION

Materials and Methods. Compounds $[HFe_2(pdt)(CO)_4(dppv)]BF_4$[16] ($[H3]BF_4$), $[HFe_2(pdt)(CO)_3(dppv)(PMe_3)]BF_4$ ($[H2]BF_4$),[33] and $[HFe_2(pdt)(CO)_2(dppv)_2]BF_4$ ($[H1]BF_4$)[21] were prepared as previously reported. Cp^*_2Co was purchased from Sigma–-Aldrich and used as received.

IR spectra were recorded on a Perkin–Elmer Spectrum 100 Fourier transform IR (FT-IR) spectrometer. Cyclic voltammetry was performed under nitrogen at room temperature using a CH Instruments CHI600D electrochemical analyzer with a glassy carbon working electrode, Pt wire counter electrode, and the pseudoreference electrode Ag wire. The sample (1 mM) and $[NBu_4]PF_6$ (100 mM) were dissolved in THF. The scan rate was 0.1 V s^{-1}, and potentials were reported relative to internal Fc/Fc^+. Microanalytical data were acquired using an Exeter Analytical CE-440 elemental analyzer. Crystallographic data were collected using a Bruker SMART equipped with a 3-circle platform diffractometer and an APEX II charge-coupled device area detector.

$[DFe_2(pdt)(CO)_2(dppv)_2]PF_6$ ($[D1]PF_6$). A solution of 160 mg (0.15 mmol) of **1** in 20 mL of CH_2Cl_2 was treated with 0.1 mL (1.29 mmol) of CF_3CO_2D (99.5 atom %D) in a glovebox. After the reaction solution stirred for 2 h, the solvent was removed under vacuum. The residue, a brown solid, was rinsed with Et_2O (10 mL × 3) and then redissolved in 5 mL of MeOH. This solution was treated with 5 mL of CH_3OH saturated with NH_4PF_6. A brown solid precipitated and was isolated by filtration. The product was washed with H_2O (10 mL × 3),

dx.doi.org/10.1021/ja312458f | J. Am. Chem. Soc. 2013, 135, 3633–3639

MeOH (10 mL × 3), and diethyl ether (10 mL × 3) and then dried under vacumn. Yield: 120 mg (66%). ^{1}H NMR (500 MHz, CD_2Cl_2): δ 7.06−7.09 (m, 40H, 40 × Ar*H*), 6.59−6.61 (m, 2H, Ph_2PCH=C*H*PPh_2), 6.33−6.36 (m, 2H, Ph_2PCH=C*H*PPh_2), 2.44−2.58 (m, 2H, S*CH*$_2$CH$_2$CH$_2$S), 1.85−2.03(m, 2H, SCH$_2$*CH*$_2$CH$_2$S), 1.54 (m, 2H, SCH$_2$C*H*$_2$CH$_2$S). ^{2}H NMR (500 MHz, CH_2Cl_2 with 1% CD_2Cl_2 as internal standard): δ −14.76 (m, μ-D). ^{31}P NMR (500 MHz, CD_2Cl_2): δ 87, 85.8 (s, *sym*-[D**1**]$^+$); δ 86, 82.2, 80.8, and 74.8 (s, *unsym*-[D**1**]$^+$); −145.0 (septet, PF_6^-). FT-IR (CH_2Cl_2, ν_{CO}): 1951 (vs), 1971 (sh) cm^{-1}.

DFe$_2$(pdt)(CO)$_2$(dppv)$_2$ ([D1]^0). Compound D**1** was prepapred by reduction of [D**1**]PF_6 following the same procedure as [H**1**]^0. Yield: 76%. FT-IR (toluene, ν_{CO}): 1892 (vs) cm^{-1}.

HFe$_2$(pdt)(CO)$_2$(dppv)$_2$ ([H1]^0). To a solution of [H**1**]BF_4 (230 mg, 0.2 mmol) in 50 mL of dry THF was added Cp*$_2$Co (73 mg, 0.22 mmol) as solid in an nitrogen box. The color of the mixture immediately changed from brown red to black, and the THF was evaporated under vacumn. The residue was extracted into toluene (20 mL × 3). The black solution was filtered through Celite, concentrated, and diluted with 20 mL of pentane, resulting in precipitation of a black solid. Yield: 154 mg (72%). FT-IR (THF, ν_{CO}): 1893 (vs) cm^{-1}. Anal. Calcd (found) for $C_{57}H_{51}Fe_2O_2P_4S_2$: C, 64.12 (63.71); H, 4.81 (5.12). Single crystals were obtained by slow vapor diffusion of pentane into a toluene solution of [H**1**]^0 at room temperature.

HER Experiments. Reactions were conducted in a tapered VWR microwave reaction vial containing a small stir bar in a glovebox. For a typical procedure, into a septum-capped vial containing 2 mL of solution of [H**1**]BF_4 (1 mM) in THF was injected with 0.1 mL of THF solution of H(OEt$_2$)$_2$BAr^F_4 (22 mM). The septum was sealed with grease and removed from the glovebox. Into the vial was injected 60 μL of methane followed by gas chromatographic analysis on a column packed with 5 Å molecular sieves (carrier gas: Ar), using an Agilent 7820A instrument equipped with a thermal conductivity detector. The response factor for H_2/CH_4 was 3.6 under our conditions, as established by calibration with known amounts of standard H_2 and CH_4. Three samples were run for this experiment. The yields for H_2 generation based on the amount of [H**1**]BF_4 were quantified as 44%, 43%, and 51%, respectivly. Thus, the average yield of H_2 was calculated to be 46% with a standard deviation σ of 0.035.

To quantify the yield of [H**1**]$^+$ for the reaction of [H**1**]^0 and D(Et$_2$O)$_2$BAr^F_4,[34] one equiv of [HFe$_2$(edt)(CO)$_4$(PMe$_3$)$_2$]PF_6 was added to the sample before ^{1}H NMR analysis. The ratio of [H**1**]$^+$ to [HFe$_2$(edt)(CO)$_4$(PMe$_3$)$_2$]PF_6 was found to be 0.99:1 by integration of the corresponding μ-H signal, indicating *no* [D**1**]$^+$ was produced.

To quantify the yield of [D**1**]$^+$ for the reaction of [D**1**]^0 and H(Et$_2$O)$_2$BAr^F_4, one equiv of [HFe$_2$(edt)(CO)$_4$(PMe$_3$)$_2$]PF_6 was added to the sample before NMR analysis. The ratio of [D**1**]$^+$ to [HFe$_2$(edt)(CO)$_4$(PMe$_3$)$_2$]PF_6 was found to be 1.95:1 by integration of the corresponding ^{31}P signal. The yield of [D**1**]$^+$ was caculated to be 97.5%. The ^{2}H NMR spectrum showed only μ-D signal of [D**1**]$^+$, while the ^{1}H NMR spectrum displayed one μ-H signal for [HFe$_2$(edt)(PMe$_3$)$_2$(CO)$_4$]$^+$. These results suggest that *only* [D**1**]$^+$ was produced and there was *no* H/D exchanges between [D**1**]$^+$ and [HFe$_2$(edt)(CO)$_4$(PMe$_3$)$_2$]$^+$.

Oxidation of [H1]^0 with CF$_3$SO$_3$Me. A reaction vial containing 5 mL of solution of [H**1**]BF_4 (47 mg, 0.044 mmol) in toluene was capped with a septum in a glovebox. The reaction mixture was treated with 1 equiv of CF_3SO_3Me (5 μL) by injection, and the spectrum was sealed with grease. The black solution turned to brown in seconds with concomitant appearance of a brown-colored solid precipitate. The gas in the headspace of the vial was sampled by syringe and analyzed by gas chromatography, which showed only a trace amount of methane. The solvent was evaporated, and the substance was dissovled in CH_2Cl_2. FT-IR (CH_2Cl_2, ν_{CO}): 1950 (vs), 1971 (sh) cm^{-1}. The ^{31}P NMR spectrum matched that for [H**1**]$^+$.

EPR Experiments. EPR samples were prepared in a MBraun glovebox. The sample concentration is approximately 2 mM in toluene. EPR spectra were recorded on a Varian E-line 12″ Century series X-band CW spectrometer. EPR spectra were simulated using the program SIMPOW6.[35]

DFT Calculations. DFT calculations were performed with ADF2012 and the ZORA Hamiltonian for relativistic effects and spin−orbit coupling implemented as described in the Supporting Information.[36]

■ ASSOCIATED CONTENT

Ⓢ Supporting Information

Crystallographic information as a CIF file; additional IR, EPR, and NMR (^{1}H, ^{2}H, ^{31}P) spectra; computational details; and a table of optimized structures and calculated EPR parameters. This material is available free of charge via the Internet at http://pubs.acs.org.

■ AUTHOR INFORMATION

Corresponding Author

rauchfuz@illinois.edu; matthias.stein@mpi-magdeburg.mpg.de

Notes

The authors declare no competing financial interest.

■ ACKNOWLEDGMENTS

This work was supported as part of the ANSER Center, an Energy Frontier Research Center funded by the U.S. Department of Energy, Office of Science, Office of Basic Energy Sciences, under award number DE-SC0001059, and the Max-Planck Society for the Advancement of Science.

■ REFERENCES

(1) Lewis, N. S.; Nocera, D. G. *Proc. Natl. Acad. Sci. U.S.A.* **2006**, *103*, 15729.

(2) Jablonskyė, A.; Wright, J. A.; Fairhurst, S. A.; Peck, J. N. T.; Ibrahim, S. K.; Oganesyan, V. S.; Pickett, C. J. *J. Am. Chem. Soc.* **2011**, *133*, 18606.

(3) Hauch, A.; Ebbesen, S. D.; Jensen, S. H.; Mogensen, M. *J. Mater. Chem.* **2008**, *18*, 2331. Holladay, J. D.; Hu, J.; King, D. L.; Wang, Y. *Catal. Today* **2009**, *139*, 244.

(4) Artero, V.; Chavarot-Kerlidou, M.; Fontecave, M. *Angew. Chem. Int. Ed.* **2011**, *50*, 7238. Dempsey, J. L.; Brunschwig, B. S.; Winkler, J. R.; Gray, H. B. *Acc. Chem. Res.* **2009**, *42*, 1995. Rakowski DuBois, M.; DuBois, D. L. *Acc. Chem. Res.* **2009**, *42*, 1974.

(5) Zaffaroni, R.; Rauchfuss, T. B.; Gray, D. L.; De Gioia, L.; Zampella, G. *J. Am. Chem. Soc.* **2012**, *134*, 19260.

(6) Barton, B. E.; Rauchfuss, T. B. *J. Am. Chem. Soc.* **2010**, *132*, 14877. Carroll, M. E.; Barton, B. E.; Gray, D. L.; Mack, A. E.; Rauchfuss, T. B. *Inorg. Chem.* **2011**, *50*, 9554. Weber, K.; Krämer, T.; Shafaat, H. S.; Weyhermuller, T.; Bill, E.; van Gastel, M.; Neese, F.; Lubitz, W. *J. Am. Chem. Soc.* **2012**, *134*, 20745.

(7) Tschierlei, S.; Ott, S.; Lomoth, R. *Energy Environ. Sci.* **2011**, *4*, 2340.

(8) Felton, G. A. N.; Mebi, C. A.; Petro, B. J.; Vannucci, A. K.; Evans, D. H.; Glass, R. S.; Lichtenberger, D. L. *J. Organomet. Chem.* **2009**, *694*, 2681.

(9) Carroll, M. E.; Barton, B. E.; Rauchfuss, T. B.; Carroll, P. J. *J. Am. Chem. Soc.* **2012**, *134*, 18843.

(10) Gloaguen, F.; Rauchfuss, T. B. *Chem. Soc. Rev.* **2009**, *38*, 100.

(11) Tard, C.; Pickett, C. J. *Chem. Rev.* **2009**, *109*, 2245.

(12) Felton, G. A. N.; Vannucci, A. K.; Okumura, N.; Lockett, L. T.; Evans, D. H.; Glass, R. S.; Lichtenberger, D. L. *Organometallics* **2008**, *27*, 4671.

(13) Eckenhoff, W. T.; Eisenberg, R. *Dalton Trans.* **2012**, *41*, 13004. Wang, M.; Chen, L.; Li, X.; Sun, L. *Dalton Trans.* **2011**, 40. Reisner, E. *Eur. J. Inorg. Chem.* **2011**, 1005.

(14) Wright, J. A.; Pickett, C. J. *Chem. Commun.* **2009**, 5719. Jablonskytė, A.; Wright, J. A.; Pickett, C. J. *Dalton Trans.* **2010**, *39*, 3026. Liu, C.; Peck, J. N. T.; Wright, J. A.; Pickett, C. J.; Hall, M. B. *Eur. J. Inorg. Chem.* **2011**, 1080.

(15) Heinekey, D. M. *J. Organomet. Chem.* **2009**, *694*, 2671.

(16) Barton, B. E.; Olsen, M. T.; Rauchfuss, T. B. *J. Am. Chem. Soc.* **2008**, *130*, 16834.
(17) Wang, M.; Chen, L.; Sun, L. *Energy Environ. Sci.* **2012**, *5*, 6763.
(18) Capon, J.-F.; Gloaguen, F.; Pétillon, F. Y.; Schollhammer, P.; Talarmin, J. *Coord. Chem. Rev.* **2009**, *253*, 1476.
(19) Keizer, P. N.; Krusic, P. J.; Morton, J. R.; Preston, K. F. *J. Am. Chem. Soc.* **1991**, *113*, 5454.
(20) Connelly, N. G.; Geiger, W. E. *Chem. Rev.* **1996**, *96*, 877.
(21) Barton, B. E.; Rauchfuss, T. B. *Inorg. Chem.* **2008**, *47*, 2261.
(22) Izutsu, K. *Acid-Base Dissociation Constants in Dipolar Aprotic Solvents*; Blackwell Scientific Publications: Oxford, U.K., 1990.
(23) Zhao, X.; Chiang, C.-Y.; Miller, M. L.; Rampersad, M. V.; Darensbourg, M. Y. *J. Am. Chem. Soc.* **2003**, *125*, 518.
(24) Masui, H.; Lever, A. B. P. *Inorg. Chem.* **1993**, *32*, 2199. Chatt, J.; Kan, C. T.; Leigh, G. J.; Pickett, C. J.; Stanley, D. R. *J. Chem. Soc., Dalton Trans.* **1980**, 2032.
(25) Krusic, P. J.; Jones, D. J.; Roe, D. C. *Organometallics* **1986**, *5*, 456.
(26) (a) Hamon, P.; Toupet, L.; Hamon, J. R.; Lapinte, C. *Organometallics* **1992**, *11*, 1429. (b) Kinney, R. A.; Saouma, C. T.; Peters, J. C.; Hoffman, B. M. *J. Am. Chem. Soc.* **2012**, *134*, 12637.
(27) (a) Olsen, M. T.; Wang, W.; Rauchfuss, T. B. Unpublished work. (b) Ekomié, A.; Lefèvre, G.; Fensterbank, L.; Lacôte, E.; Malacria, M.; Ollivier, C.; Jutand, A. *Angew. Chem., Int. Ed.* **2012**, *51*, 6942. (c) Chiang, K. P.; Scarborough, C. C.; Horitani, M.; Lees, N. S.; Ding, K.; Dugan, T. R.; Brennessel, W. W.; Bill, E.; Hoffman, B. M.; Holland, P. L. *Angew. Chem., Int. Ed.* **2012**, *51*, 3658.
(28) (a) Foerster, S.; Gastel, M. v.; Brecht, M.; Lubitz, W. *J. Biol. Inorg. Chem.* **2005**, *10*, 51. (b) Brecht, M.; van Gastel, M.; Buhrke, T.; Friedrich, B.; Lubitz, W. *J. Am. Chem. Soc.* **2003**, *125*, 13075.
(29) Pandelia, M.-E.; Infossi, P.; Stein, M.; Giudici-Orticoni, M.-T.; Lubitz, W. *Chem. Commun.* **2012**, *48*, 823.
(30) Ezzaher, S.; Capon, J.-F.; Dumontet, N.; Gloaguen, F.; Pétillon, F. Y.; Schollhammer, P.; Talarmin, J. *J. Electroanal. Chem.* **2009**, *626*, 161.
(31) Marinescu, S. C.; Winkler, J. R.; Gray, H. B. *Proc. Natl. Acad. Sci. U.S.A.* **2012**, *109*, 15127.
(32) Apfel, U.-P.; Troegel, D.; Halpin, Y.; Tschierlei, S.; Uhlemann, U.; Görls, H.; Schmitt, M.; Popp, J.; Dunne, P.; Venkatesan, M.; Coey, M.; Rudolph, M.; Vos, J. G.; Tacke, R.; Weigand, W. *Inorg. Chem.* **2010**, *49*, 10117.
(33) Barton, B. E.; Zampella, G.; Justice, A. K.; De Gioia, L.; Rauchfuss, T. B.; Wilson, S. R. *Dalton Trans.* **2010**, *39*, 3011.
(34) Brookhart, M.; Grant, B.; Volpe, A. F. *Organometallics* **1992**, *11*, 3920.
(35) Nilges, M. J.; Matteson, K.; Belford, R. L. SIMPOW6: a software package for the simulation of ESR powerder-type spectra. In *ESR Spectroscopy in Membrane Biophysics, Biological Magnetic Resonance*; Hemminga, M. A., Berliner, L., Eds.; Springer: New York, 2007.
(36) (a) Scientific Computing & Modelling. *ADF*; Vrije Universiteit, Theoretical Chemistry: Amsterdam, The Netherlands, 2012. (b) te Velde, G.; Bickelhaupt, F. M.; Baerends, E. J.; Guerra, C. F.; Van Gisbergen, S. J. A.; Snijders, J. G.; Ziegler, T. *J. Comput. Chem.* **2001**, *22*, 931.